Inorganic Chemistry

Article

pubs.acs.org/IC

New Mixed-Valent Mn Clusters from the Use of *N,N,N′,N′*-Tetrakis(2-hydroxyethyl)ethylenediamine ($edteH_4$): Mn_3, Mn_4, Mn_6, and Mn_{10}

Arpita Saha, Khalil A. Abboud, and George Christou*

Department of Chemistry, University of Florida, Gainesville, Florida 32611-7200, United States

Supporting Information

ABSTRACT: The syntheses, crystal structures, and magnetochemical characterization are reported for the new mixed-valent Mn clusters $[Mn_2^{II}Mn^{III}(O_2CMe)_2(edteH_2)_2](ClO_4)$ (**1**), $[Mn^{II}_2Mn^{III}_2(edteH_2)_2(hmp)_2Cl_2](Mn^{II}Cl_4)$ (**2**), $[Mn^{III}_6O_2(O_2CBu^t)_6(edteH)_2(N_3)_2]$ (**3**), $[Na_2Mn^{III}_8Mn^{II}_2O_4(OMe)_2(O_2CEt)_6(edte)_2(N_3)_6]$ (**4**), and $(NEt_4)_2[Mn_8^{III}Mn_2^{II}O_4(OH)_2(O_2CEt)_6(edte)_2(N_3)_6]$(**5**), where $edteH_4$ is *N,N,N′,N′*-tetrakis-(2-hydroxyethyl)ethylenediamine and hmpH is 2-(hydroxymethyl)pyridine. **1**−**5** resulted from a systematic exploration of the effect of different Mn sources, carboxylates, the presence of azide, and other conditions, on the Mn/$edteH_4$ reaction system. The core of **1** consists of a linear $Mn^{II}Mn^{III}Mn^{II}$ unit, whereas that of **2** is a planar Mn_4 rhombus within a $[Mn^{II}_2Mn^{III}_2(\mu_3\text{-OR})_2]$ incomplete-dicubane unit. The core of **3** comprises a central $[Mn^{III}_4(OR)_2]$ incomplete-dicubane on either side of which is edge-fused a triangular $[Mn^{III}_3(\mu_3\text{-O})]$ unit. The cores of **4** and **5** are similar and consist of a central $[Mn^{II}_2Mn^{III}_2(\mu_3\text{-OR})_2]$ incomplete-dicubane on either side of which is edge-fused a distorted $[Mn^{II}Mn^{III}_3(\mu_3\text{-O})_2(\mu_3\text{-OR})_2]$ cubane unit. Variable-temperature, solid-state direct current (dc) and alternating current (ac) magnetization studies were carried out on **1**−**5** in the 5.0−300 K range, and they established the complexes to have ground state spin values of $S = 3$ for **1**, $S = 9$ for **2**, and $S = 4$ for **3**. The study of **3** provided an interesting caveat of potential pitfalls from particularly low-lying excited states. For **4** and **5**, the ground state is in the $S = 0$−4 range, but its identification is precluded by a high density of low-lying excited states.

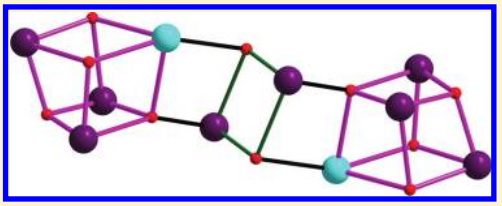

INTRODUCTION

Polynuclear Mn cluster chemistry at intermediate oxidation states (Mn^{II}−Mn^{IV}) continues to attract much attention from groups around the world for its relevance to various areas such as bioinorganic chemistry and molecular nanoscience, as well as for the aesthetically pleasing structures it often produces. In Mn bioinorganic chemistry, the occurrence of Mn atoms at the active sites of a variety of redox enzymes such as the oxygen-evolving center (OEC) within the Photosystem II reaction center of plants and cyanobacteria is an active area of study;[1,2] the active site of the OEC is now confirmed to be a pentanuclear $CaMn_4$ cluster.[3] From the nanoscience viewpoint, Mn complexes are of particular interest for their magnetic properties: they often display large ground state spin (S) values as a result of ferromagnetic exchange interactions and/or spin frustration effects,[4,5] and if such large S values are coupled with significant magnetoanisotropy of the Ising (easy-axis) type, then such molecules have the potential to be single-molecule magnets (SMMs).[6] The latter are individual molecules that possess a significant barrier (vs kT) to magnetization relaxation, and they can consequently function as nanoscale magnets below their blocking temperature (T_B), which thus represents a molecular approach to nanomagnetism. In contrast, when they possess little or no anisotropy, they are of interest as components for molecule-based magnetic refrigeration based on the magnetocaloric effect.[7]

As a result of the above, there continues to be a need to develop new synthetic procedures to polynuclear Mn clusters. One approach we have been investigating recently is to take ligands that are known to yield such compounds and modify them by introducing bulky groups that divert the reaction to different structural types of product.[8] Another is to explore new poly alcohol groups to foster formation of high nuclearity products. Along these lines, we have recently been exploring the use in Mn carboxylate chemistry of the potentially O,O,O,O,N,N hexadentate chelate *N,N,N′,N′*-tetrakis-(2-hydroxyethyl)ethylenediamine ($edteH_4$) whose protonated arms could each form bridges between multiple metal atoms.The $edteH_4$ group has been little explored to date in the literature, having been originally employed only in the preparation of mononuclear Ca and dinuclear Ba, Cu, and V complexes.[9] In initial work with Mn, however, $edteH_4$ has given Mn_8, Mn_{12}, and Mn_{20} complexes with new metal topologies.[10] Similarly, in Fe chemistry it has yielded new Fe_4, Fe_5, Fe_6, and Fe_{12} clusters.[10c,11] With the potential of $edteH_4$ to give new cluster types established by this early work, we have been extending its use to many other Mn reaction systems under different conditions, some also involving azide ions or another chelating group. Herein, we report a number of results from this study, the syntheses, crystal structures, and magnetic

Received: September 1, 2011
Published: November 9, 2011

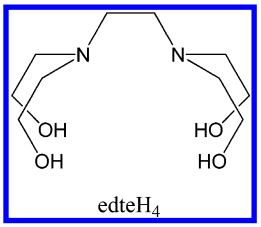

properties of a variety of new mixed-valence $Mn^{II,III}_x$ complexes spanning nuclearities Mn_3, Mn_4, Mn_6, and Mn_{10}.

EXPERIMENTAL SECTION

Syntheses. All preparations were performed under aerobic conditions using reagents and solvents as received. $[Mn_8O_{10}(O_2CMe)_6(H_2O)_2(bpy)_6](ClO_4)_4$,[12] $Mn(O_2CBu^t)_2$,[13] and $Mn(O_2CEt)_2$[14] were prepared as reported in the literature. ***Caution!*** *Although no such behavior was observed during the present work, azide salts are potentially explosive; such compounds should be synthesized and used in small quantities, and treated with utmost care at all times.*

$[Mn_3(O_2CMe)_2(edteH_2)_2](ClO_4)$ (1). To a stirred solution of $edteH_4$ (0.05 g, 0.21 mmol) in MeCN/MeOH (10/1, v/v) was added $[Mn_8O_{10}(O_2CMe)_6(H_2O)_2(bpy)_6](ClO_4)_4$ (0.10 g, 0.04 mmol). The resulting dark-brown solution was stirred for 6 h, filtered, and then Et_2O was slowly added to the filtrate by vapor diffusion. X-ray quality reddish-brown plate-like crystals of **1**·MeCN grew over 12 days in a yield of ∼50%. The crystals were collected by filtration, washed with Et_2O, and dried in vacuum. Anal. Calcd (Found) for **1**·H_2O: C: 32.50 (32.35); H: 6.14 (5.76); N: 6.32 (6.45). Selected IR data (cm^{-1}): 2977(m), 2857(m), 1570(s), 1405(m), 1094(vs), 912(m), 733(w), 650(m), 625(m), 586(m), 543(m), 508(m).

$[Mn_4(edteH_2)_2(hmp)_2Cl_2](MnCl_4)$ (2). To a stirred solution of $edteH_4$ (0.10 g, 0.42 mmol) and NEt_3 (0.06 mL, 0.42 mmol) in MeOH (12 mL) was added $MnCl_2$ (0.17 g, 0.84 mmol). The resulting dark-brown solution was stirred for 30 min and then hmpH (0.20 mL, 2.1 mmol) was added and the solution stirred for a further 2 h. The solution was filtered, and the filtrate layered with Et_2O. X-ray quality, dark-brown hexagonal plate-like crystals of **2** grew over 15 days in a yield of 12%. The crystals were collected by filtration, washed with Et_2O, and dried in vacuum. Anal. Calcd (Found) for **2**: C: 32.79 (33.24); H: 4.82 (4.88); N: 7.17 (6.87). Selected IR data (cm^{-1}): 2937(m), 2677(m), 2492(m), 1608(s), 1475(s), 1439(s), 1397(w), 1289(w), 1171(w), 1063(vs), 925(m), 771(m), 731(w), 665(br), 519(br).

$[Mn_6O_2(O_2CBu^t)_6(edteH)_2(N_3)_2]$ (3). To a stirred solution of $edteH_4$ (0.20 g, 0.84 mmol) and NEt_3 (0.24 mL, 1.68 mmol) in MeCN (20 mL) was added $Mn(O_2CBu^t)_2$ (0.60 g, 2.29 mmol). The resulting dark-brown solution was stirred for 15 min under mild heating (∼60 °C) to dissolve all solids, and then Me_3SiN_3 (0.4 mL, 3.01 mmol) was added and the solution stirred for a further 2 h. The solution was filtered, and the filtrate left to slowly evaporate undisturbed at ∼4 °C. X-ray quality, dark-brown plate-like crystals of **3** grew over 10 days in a yield of 24%. The crystals were collected by filtration, washed with Et_2O, and dried in vacuum. Anal. Calcd (Found) for **3**: C: 39.54 (39.71); H: 6.37 (6.68); N: 9.22 (9.45). Selected IR data (cm^{-1}): 3395(br), 2957(vs), 2899(s), 2863(s), 2067(vs), 1586(vs), 1482(s), 1415(s), 1359(s), 1225(s), 1086(vs), 919(m), 897(m), 787(w), 695(s), 587(vs), 508(m), 417(w).

$[Na_2Mn_{10}O_4(OMe)_2(O_2CEt)_6(edte)_2(N_3)_6]$ (4). To a stirred solution of $edteH_4$ (0.15 g, 0.64 mmol) and LiOH (0.06 g, 0.64 mmol) in MeCN/MeOH (10/5, v/v) was added $Mn(O_2CEt)_2$ (0.34 g, 1.28 mmol). The resulting dark-brown solution was stirred for 1 h and then NaN_3 (0.33 g, 5.12 mmol) was added and the solution stirred for a further 3 h. The solution was filtered, and the filtrate left undisturbed to slowly evaporate. X-ray quality, dark-brown plate-like crystals of **4**·2MeCN grew over 14 days in a yield of 80%. The crystals were collected by filtration, washed with Et_2O, and dried in vacuum. Anal. Calcd (Found) for **4**·2H_2O: C: 25.12 (25.05); H: 4.22 (4.06); N: 16.11 (16.14). Selected IR data (cm^{-1}): 2980(m), 2867(m), 2050(vs),1557(s), 1412(m), 1291(m), 1062(s), 911(m), 558(br).

$(NEt_4)_2[Mn_{10}O_4(OH)_2(O_2CEt)_6(edte)_2(N_3)_6]$ (5). To a stirred solution **4** (0.10 g, 0.1 mmol) in MeCN (6 mL) was added NEt_4Cl (0.02 g, 0.2 mmol). The resulting dark-brown solution was stirred for 1 h, filtered, and Et_2O slowly added to the filtrate by vapor diffusion. X-ray quality, dark-brown, plate-like crystals of **5**·2MeCN grew over a few days in a yield of 40%. The crystals were collected by filtration, washed with Et_2O, and dried in vacuum. Anal. Calcd (Found) for **5**·H_2O: C: 31.17 (30.91); H: 5.52 (5.51); N: 16.15 (16.54). Selected IR data (cm^{-1}): 2980(m), 2062(s), 1635(m), 1558(m), 1396(m), 1290(m), 1072(m), 911(m), 558(br).

X-ray Crystallography. Data were collected on a Siemens SMART PLATFORM equipped with a CCD area detector and a graphite monochromator utilizing Mo−Kα radiation (λ = 0.71073 Å). Suitable crystals were attached to glass fibers using silicone grease and transferred to a goniostat where they were cooled to 173 K for data collection. Cell parameters were refined using 8192 reflections. A full sphere of data (1850 frames) was collected using the ω-scan method (0.3° frame width). The first 50 frames were remeasured at the end of data collection to monitor instrument and crystal stability (maximum correction on I was <1%). Absorption corrections by integration were applied based on measured indexed crystal faces. The structure was solved by direct methods in SHELXTL6, and refined on F^2 using full-matrix least-squares. The non-H atoms were treated anisotropically, whereas the H atoms were placed in ideal, calculated positions and were refined as riding on their respective C atoms.

For **1**·MeCN, the asymmetric unit consists of two half Mn_3 cations, a ClO_4^- anion, and an MeCN solvent molecule. The latter was too disordered to be modeled properly, thus program SQUEEZE,[15] a part of the PLATON package of crystallographic software, was used to remove its contribution to the overall intensity data. A total of 16312 parameters were refined in the final cycle of refinement using 4676 reflections with $I > 2\sigma(I)$ to yield R_1 and wR_2 of 3.72 and 9.79%, respectively. For **2**, the asymmetric unit consists of one Mn_4 cation, and a $MnCl_4^-$ anion. A total of 267 parameters were refined in the final cycle of refinement using 4499 reflections with $I > 2\sigma(I)$ to yield R_1 and wR_2 of 4.19 and 11.44%, respectively (Table 1). For **3**, the asymmetric unit consists of a half Mn_6 cluster located on an inversion center. The proton on O11, the uncoordinated hydroxyl group, was located from a difference Fourier map and was held riding on its parent atom. A total of 407 parameters were refined in the final cycle of refinement using 2883 reflections with $I > 2\sigma(I)$ to yield R_1 and wR_2 of 5.30 and 11.24%, respectively. For **4**·2MeCN, the asymmetric unit

Table 1. Crystallographic Data for 1·MeCN and 2

parameter	1	2
formula	$C_{24}H_{50}ClMn_3N_4O_{16}$	$C_{32}H_{52}Cl_6Mn_5N_6O_{10}$
fw, g/mol	850.95	1168.2
crystal system	monoclinic	monoclinic
space group	$P2_1/n$	$C2/c$
a, Å	15.762(4)	26.757(2)
b, Å	14.032(4)	10.7825(9)
c, Å	17.582(5)	15.7930(13)
β,	113.187(4)	91.931(2)
Z	4	8
T, K	100(2) K	173(2)
radiation, Å[a]	0.71073	0.71073
ρ, g/cm^3	1.581	1.704
μ, mm^{-1}	1.191	1.758
R1[b,c]	0.0372	0.0419
wR2[d]	0.0979	0.1144

[a]Graphite monochromator. [b]$I > 2\sigma(I)$. [c]$R1 = \sum||F_o| - |F_c||/\sum|F_o|$. [d]$wR2 = [\sum w(F_o^2 - F_c^2)^2/\sum w(F_o^2)^2]^{1/2}$, $w = 1/[\sigma^2(F_o^2) + [(ap)^2 + bp]$, where $p = [F_o^2 + 2F_c^2]/3$.

dx.doi.org/10.1021/ic201916d | Inorg. Chem. 2011, 50, 12774–12784

consists of a half Mn_{10} cluster and a MeCN solvent molecule. A total of 523 parameters were refined in the final cycle of refinement using 7541 reflections with $I > 2\sigma(I)$ to yield R_1 and wR_2 of 4.17 and 11.07%, respectively (Table 2). For **5**·2MeCN, the asymmetric unit consists of two half Mn_{10} anions, two NEt_4^+ cations, and two MeCN solvent molecules. Each half cluster has two disorders: One is a hydroxyl ligand disordered against an azide ligand. For the other, the CH_2 on N1 and N1′ of an edte ligand are disordered and refined in two parts. A check for higher symmetry was performed but none exists. One MeCN molecule is disordered alongside the OH^-/N_3^- disorder. A total of 1086 parameters were refined in the final cycle of refinement using 14604 reflections with $I > 2\sigma(I)$ to yield R_1 and wR_2 of 4.03 and 8.96%, respectively.

Table 2. Crystallographic Data for 3, 4·2MeCN, and 5·2MeCN

parameter	3	4	5
formula	$C_{50}H_{94}Mn_6N_{10}O_{22}$	$C_{50}H_{94}Mn_{10}N_{26}Na_2O_{28}$	$C_{58}H_{117.50}Mn_{10}N_{27.5}O_{25.5}$
fw, g/mol	1517.0	2102.9	2157.70
crystal system	monoclinic	triclinic	triclinic
space group	$C2/c$	$P\bar{1}$	$P\bar{1}$
a, Å	23.5084(17)	12.682(2)	13.058(3)
b, Å	14.4661(11)	12.716(2)	16.551(3)
c, Å	20.2570(15)	14.595(3)	22.339(5)
α, deg	90	90.132(4)	82.451(4)
β, deg	104.264(5)	96.501(3)	82.488(7)
γ, deg	90	115.491(3)	66.784(7)
V, Å^3	6676.5(9)	2107.5(7)	4382.3(16)
Z	8	2	2
T, K	100(2) K	173(2)	100(2) K
radiation, Å[a]	0.71073	0.71073	0.71073
ρ, g/cm^3	1.509	1.657	1.635
μ, mm^{-1}	9.620	1.541	1.474
R1[b,c]	0.0530	0.0417	0.0403
wR2[d]	0.1124	0.1107	0.0896

[a]Graphite monochromator. [b]$I > 2\sigma(I)$. [c]$R1 = \sum||F_o| - |F_c||/\sum|F_o|$. [d]$wR2 = [\sum w(F_o^2 - F_c^2)^2/\sum w(F_o^2)^2]^{1/2}$, $w = 1/[\sigma^2(F_o^2) + [(ap)^2 + bp]$, where $p = [F_o^2 + 2F_c^2]/3$.

Physical Measurements. Infrared spectra were recorded in the solid state (KBr pellets) on a Nicolet Nexus 670 FTIR spectrometer in the 400−4000 cm^{-1} range. Elemental analyses (C, H, and N) were performed by the in-house facilities of the University of Florida, Chemistry Department. Variable-temperature direct current (dc) and alternating current (ac) magnetic susceptibility data were collected at the University of Florida using a Quantum Design MPMS-XL SQUID magnetometer equipped with a 7 T magnet and operating in the 1.8−300 K range. Samples were embedded in solid eicosane to prevent torquing. Magnetization vs field and temperature data were fit using the program MAGNET.[16] Pascal's constants were used to estimate the diamagnetic correction, which was subtracted from the experimental susceptibility to give the molar paramagnetic susceptibility (χ_M).

RESULTS AND DISCUSSION

Syntheses. Two methods have been employed in this work to prepare Mn^{III}-containing clusters from $edteH_4$: one is the reaction with preformed higher oxidation state Mn_x clusters[17] and the second is to use Mn^{II} reagents and oxidize them with atmospheric O_2.[18] In both cases, many reaction systems under various conditions, many also including azide ions, were explored before the following procedures were developed. The reaction of $[Mn_8O_{10}(O_2CMe)_6(H_2O)_2(bpy)_6](ClO_4)_4$ with $edteH_4$ in a 1:5 molar ratio in MeCN, with or without added NEt_3, led to $[Mn_3(O_2CMe)_2(edteH_2)_2](ClO_4)$ (**1**; $Mn_2^{II}Mn^{III}$) in ∼50% yield. The high yield suggests the slight excess of $edteH_4$ provides reducing equivalents to lower the Mn oxidation level from +3.75 in the Mn_8 reagent to +2.33 in **1**; the reaction is summarized in eq 1.

$$3[Mn_8O_{10}(O_2CMe)_6(H_2O)_2(bpy)_6]^{4+} + 16edteH_4 + 30H^+ + 34e^- \rightarrow 8[Mn_3(O_2CMe)_2(edteH_2)_2]^+ + 2MeCO_2H + 18bpy + 36H_2O \quad (1)$$

The use of simple Mn^{2+} salts as starting materials in the presence of azide or hmpH led to products of higher nuclearity than **1**. Both end-on azide and hmp^- bridges are known to give ferromagnetic coupling, so we anticipated that their incorporation might give magnetically interesting products.[19] The reaction of $MnCl_2$ with $edteH_4$, NEt_3 (or NMe_4OH), and hmpH in a 2:1:1:5 molar ratio in MeOH afforded a reddish-brown solution from which was subsequently obtained $[Mn_2^{II}Mn^{III}(O_2CMe)_2(edteH_2)_2](Mn^{II}Cl_4)$ (**2**) in low (12%) yield. The reaction was clearly a messy one, and we were unable to obtain any other pure products from the filtrate. The formation of **2** is summarized in eq 2, where atmospheric O_2 is assumed to provide the oxidizing equivalents.

$$5MnCl_2 + 2edteH_4 + 2hmpH + \frac{1}{2}O_2 \rightarrow [Mn_4(edteH_2)_2(hmp)_2Cl_2][MnCl_4] + 4HCl + H_2O \quad (2)$$

To preclude the presence of $MnCl_4^{2-}$, various Mn^{II} carboxylate salts were employed. The reaction between $Mn(O_2CBu^t)_2$, $edteH_4$, NEt_3, and Me_3SiN_3 was explored, the Me_3SiN_3 being preferred to NaN_3 to avoid the presence of Na^+ (vide infra).[20] The reaction with a ∼3:1:2:4 molar ratio led to $[Mn_6O_2(O_2CBu^t)_6(edteH)_2(N_3)_2]$ (**3**; $6Mn^{III}$) in 24% isolated yield (eq 3).

$$6Mn(O_2CBu^t)_2 + 2edteH_4 + 2Me_3SiN_3 + \frac{3}{2}O_2 \rightarrow [Mn_6O_2(O_2CBu^t)_6(edteH)_2(N_3)_2] + 2Me_3SiO_2CBu^t + 4Bu^tCO_2H + H_2O \quad (3)$$

The same product was obtained with NMe_4OH instead of NEt_3. Corresponding reactions with the smaller carboxylate, $EtCO_2^-$, were also explored, and the reaction between $Mn(O_2CEt)_2$, $edteH_4$, LiOH, and NaN_3 in a 2:1:1:8 ratio in MeCN/MeOH gave a particularly clean reaction and isolation of polymeric $[Na_2Mn_{10}O_4(OMe)_2(O_2CEt)_6(edte)_2(N_3)_6]$ (**4**; $Mn_2^{II}Mn^{III}{}_{10}$) in 80% yield (eq 4).

$$10Mn(O_2CEt)_2 + 2edteH_4 + 6NaN_3 + 2MeOH + 2O_2 \rightarrow [Na_2Mn_{10}O_4(OMe)_2(O_2CEt)_6(edte)_2(N_3)_6] + 10EtCO_2H + 4NaO_2CEt \quad (4)$$

The same product was obtained using NaOH instead of LiOH, or MeOH as solvent, but in slightly lower purity. Methods of breaking down polymer **4** into molecular units were also explored and developed from the reaction of preformed **4** with 2 equiv of NEt_4Cl in MeCN. This led to precipitation of NaCl and subsequent isolation of $(NEt_4)_2[Mn_{10}O_4(OH)_2(O_2CEt)_6(edte)_2(N_3)_6]$ (**5**), the anion of which is the Mn_{10} unit of **4**, albeit with hydrolysis of the MeO^-

dx.doi.org/10.1021/ic201916d | Inorg. Chem. 2011, 50, 12774–12784

bridges to OH^- (eq 5).

$$[Na_2Mn_{10}O_4(OMe)_2(O_2CEt)_6(edte)_2(N_3)_6] + 2NEt_4Cl + 2H_2O \rightarrow (NEt_4)_2[Mn_{10}O_4(OH)_2(O_2CEt)_6(edte)_2(N_3)_6] + 2NaCl + 2MeOH \quad (5)$$

Description of Structures. The structure of the $[Mn_3(O_2CMe)_2(edteH_2)_2]^+$ cation of **1** is shown in Figure 1,

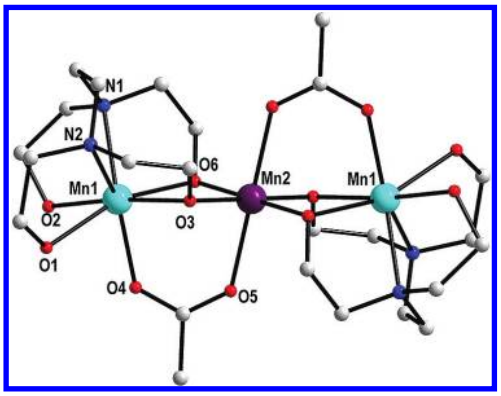

Figure 1. Structure of the cation of **1**. H atoms have been omitted for clarity. Color code: Mn^{III}, purple; Mn^{II}, cyan; O, red; N, blue; C, light gray.

and selected interatomic distances and angles are summarized in Table 3. The cation lies on an inversion center and contains

Table 3. Selected Interatomic Distances (Å) and Angles (deg) for 1·MeCN

Mn(1)···Mn(2)	3.144(1)	Mn(1)–O(2)	2.308(3)
Mn(1)–O(3)	2.163(2)	Mn(1)–O(4)	2.160(2)
Mn(1)–O(6)	2.235(2)	Mn(1)–N(1)	2.374(3)
Mn(1)–O(1)	2.334(2)	Mn(1)–N(2)	2.386(3)
Mn(2)–O(3)	1.907(2)	Mn(2)–O(5)	2.250(2)
Mn(2)–O(6)	1.931(2)		
Mn(1)–O(3)–Mn(2)	100.95(10)	Mn(1)–O(6)–Mn(2)	97.73(9)

a linear $Mn^{II}Mn^{III}Mn^{II}$ unit. Each $edteH_2^{2-}$ is a hexadentate chelate on a Mn^{II} atom, Mn1, with the two protonated alcohol arms bound terminally and the two deprotonated alkoxide arms bridging to the central Mn^{III} atom, Mn2. Each $Mn^{II}Mn^{III}$ pair is also bridged by an $\eta^1{:}\eta^1{:}\mu$-acetate group, completing seven and six coordination at Mn1 and Mn2, respectively. The Mn oxidation states were obvious from the metric parameters and the Jahn–Teller (JT) axial elongation at the central Mn^{III} atom, and were confirmed by bond valence sum (BVS) calculations (Table 4).[21] Similarly, the protonation levels of the O atoms were confirmed by O BVS calculations (Supporting Information, Table S1).[22]

Inspection of the crystal packing of **1**·MeCN shows that the Mn_3 cations are connected into zig-zagging chains by O–H···O hydrogen-bonds involving the protonated OH arms of $edteH_2^{2-}$ groups on one Mn_3 unit and bridging acetate ligands on the adjacent one (Supporting Information, Figure S1).[22]

The linear $Mn^{II}{}_2Mn^{III}$ core of **1** is rare in the literature, being seen before only in two examples, one of which is an SMM.[23,24] There are also several other linear Mn_3 units at other oxidation states, including $Mn^{II}{}_3$,[25] $Mn^{II}Mn^{III}{}_2$,[26] $Mn^{II}Mn^{III}Mn^{IV}$,[27] and $Mn^{IV}{}_3$.[28]

Table 4. Bond-Valence Sums for the Mn Atoms of Complexes 1–5[a]

complex	atom	Mn^{II}	Mn^{III}	Mn^{IV}
1	Mn1	1.62	1.51	1.48
	Mn2	3.40	3.14	3.08
2	Mn1	2.04	1.90	1.91
	Mn2	3.33	3.11	3.05
	Mn3	2.08	2.14	2.08
3	Mn1	3.14	2.93	2.86
	Mn2	3.44	3.21	3.13
	Mn3	3.46	3.19	3.13
4	Mn1	2.03	1.89	1.85
	Mn2	3.36	3.09	3.04
	Mn3	3.44	3.17	3.11
	Mn4	3.36	3.14	3.06
	Mn5	3.28	3.09	3.06
5	Mn1	2.02	1.88	1.84
	Mn2	3.29	3.09	3.00
	Mn3	3.35	3.09	3.03
	Mn4	3.31	3.05	2.99
	Mn5	3.33	3.10	3.03

[a]The underlined value is the closest to the charge for which it was calculated. The oxidation state is the nearest whole number to the underlined value.

The structure of the $[Mn_4(edteH_2)_2(hmp)_2Cl_2]^{2+}$ cation of **2** is shown in Figure 2, and selected interatomic distances and

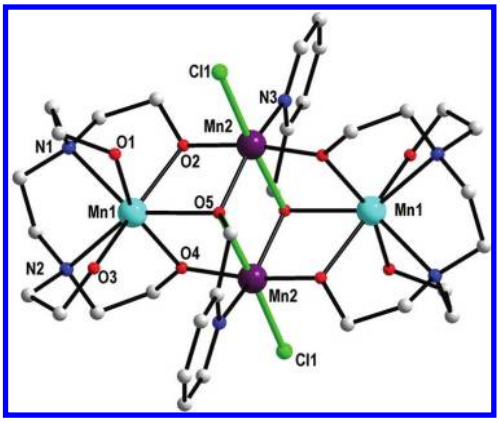

Figure 2. Structure of the cation of **2**. The Mn^{III} JT axes are shown as green lines. H atoms have been omitted for clarity. Color code: Mn^{III}, purple; Mn^{II}, cyan; O, red; N, blue; Cl, green; C, light gray.

angles are listed in Table 5. The centrosymmetric cation consists of a planar $Mn^{II}{}_2Mn^{III}{}_2$ rhombus, with each triangular unit bridged by a μ_3-O atom (O5) from the alkoxide arm of an hmp^- group that is chelating to each Mn^{III} atom, Mn2. As for **1** and **2**, each $edteH_2^{2-}$ is a hexadentate chelate on the Mn^{II} atoms, Mn1, with the two deprotonated alkoxide arms bridging to a Mn^{III} atom. Finally, a Cl^- ion on each Mn^{III} atom completes the ligation. As a result, the Mn^{II} and Mn^{III} atoms, Mn1 and Mn2, are seven- and six-coordinate, respectively. The Mn oxidation states and O protonation levels were again confirmed by BVS calculations (Table 4 and Supporting Information, Table S1). As expected, the Mn^{III} atom Mn2 exhibits a JT axial elongation, along the O5–Mn2–Cl1 axis. The crystal packing reveals intermolecular OH···Cl hydrogen-bonds between the OH groups of $edteH_2^{2-}$ groups and the $MnCl_4^{2-}$ anions (O3···Cl3 = 3.070 Å). These serve to link

dx.doi.org/10.1021/ic201916d | Inorg. Chem. 2011, 50, 12774–12784

Table 5. Selected Interatomic Distances (Å) and Angles (deg) for 2 and 3

2		3	
Mn1···Mn2	3.275(1)	Mn(1)···Mn(2)	3.014(1)
Mn(1)−O(1)	2.311(2)	Mn(2)···Mn(3)	3.267(1)
Mn(1)−O(2)	2.188(2)	Mn(1)···Mn(3)	3.320(1)
Mn(1)−O(3)	2.224(2)	Mn(1)−O(1)	1.948(3)
Mn(1)−O(4)	2.174(2)	Mn(1)−O(9)	2.671(4)
Mn(1)−O(5)	2.261(2)	Mn(1)−O(8)	1.901(4)
Mn(1)−N(1)	2.335(2)	Mn(1)−O(10)	1.953(4)
Mn(1)−N(2)	2.378(2)	Mn(2)−O(1)	1.869(3)
Mn(2)−O(4)	1.863(2)	Mn(2)−O(8)	2.239(4)
Mn(2)−O(5)	2.281(2)	Mn(3)−O(9)	2.111(4)
Mn(2)−N(3)	2.093(2)	Mn(1)−O(1)−Mn(2)	104.31(15)
Mn(2)−Cl(1)	2.449(1)	Mn(2)−O(1)−Mn(3)	123.07(19)
Mn(2)−O(4)−Mn(1)	110.19(9)	Mn(3)−O(1)−Mn(1)	122.03(18)
Mn(1)−O(5)−Mn(2)	93.77(7)	Mn(1)−O(8)−Mn(2)	93.09(15)
Mn(1)−O(2)−Mn(2′)	107.24(9)	Mn(3)−O(9)−Mn(3′)	102.24(15)
		Mn(3′)-O(10)−Mn(1)	118.69(18)

neighboring cations and anions into a chain (Supporting Information, Figure S2).[22] There are a large number of Mn_4 clusters known in the literature, spanning a wide range of metal topologies, but this is the first example with an $edteH_2^{2-}/hmp^-$ mixed chelate system.

The partially labeled structure of $[Mn^{III}_6O_2(O_2CBu^t)_6(edteH)_2(N_3)_2]$ (**3**) and a stereoview are presented in Figure 3, and selected interatomic distances and angles are listed in Table 5. The core of the centrosymmetric complex consists of two $[Mn_3(\mu_3\text{-}O^{2-})]^{7+}$ triangular units bridged by four μ-OR^- (O9, O10) groups, where the latter are deprotonated alkoxide arms of $edteH^{3-}$ groups. Alternatively, the core can be described as a central Mn_4 rhombus as in **2**, except that two opposite edges are each bridged by an O^{2-} ion rather than an alkoxide, and each of the former also bridge to Mn2. Mn1 and Mn2 are further bridged by another $edteH^{3-}$ alkoxide arm (O8), and peripheral ligation is completed by six bridging $Bu^tCO_2^-$ and two terminal N_3^- groups. Each μ_4-$edteH^{3-}$ group is now only a tetradentate chelate to one Mn atom (Mn1) with its deprotonated arms bridging a total of four Mn atoms; the protonated arm is unbound.

All six Mn^{III} ions are six-coordinate and JT elongated, and their oxidation states and O protonation levels were confirmed by BVS calculations (Tables 3 and 4). Atom Mn1 forms a long contact to alkoxide O atom O9 (Mn1···O9 = 2.671 Å), which we hesitate to consider as a true bonding interaction to make Mn1 seven-coordinate. However, this contact does have the effect of significantly distorting the Mn1 geometry from octahedral, particularly the O1−Mn1−O10 angle, which is 114.77° rather than ∼90°. A variety of Mn_6 compounds have been reported in the literature, and some can be described as two linked trinuclear units, as in **3**. Representative examples include the family of $[Mn^{III}_6O_2(R\text{-}sao)_6X_2(MeOH)_{4-6}]$ (R = H, Me, Et or Ph; X = carboxylate, O_2PHPh or O_2PPh_2) clusters,[29] $[Mn^{III}_2Mn^{II}_4(^tBuCO_2)_8(tmp)_2(py)_2]$ ($tmpH_3$ = 1,1,1-tris-(hydroxymethyl)propane),[30a] $[Mn_6(O_2CMe)_6(thme)_2(H_2tea)_2]$ ($thmeH_3$ = 1,1,1-tris-(hydroxymethyl)ethane) and $teaH_3$ = triethanolamine),[30b] and $[Mn_6O_2(O_2CMe)_{10}(RCO_2H)_2]$.[30c]

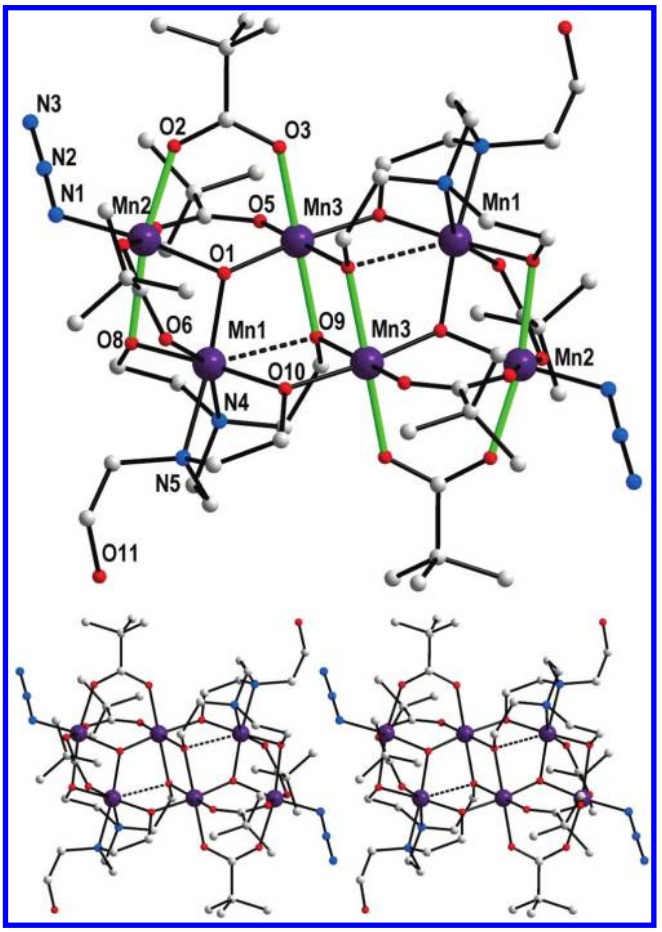

Figure 3. Structure of **3** (top) and a stereopair (bottom). The Mn^{III} JT axes are shown as green lines. The long Mn1−O9 interaction is shown as dashed lines. H atoms have been removed for clarity. Color code: Mn^{III}, purple; O, red; N, blue; C, light gray.

The partially labeled structure, a stereoview, and the core of $[Na_2Mn_{10}O_4(OMe)_2\text{-}(O_2CEt)_6(edte)_2(N_3)_6]_n$ (**4**) are presented in Figure 4, and selected interatomic distances and angles are listed in Table 6. The centrosymmetric Mn_{10} unit consists of a central Mn_4 rhombus, as in **2** and **3**, fused on each side to a distorted $[Mn_4O_2(OR)_2]^{5+}$ cubane as shown in Figure 4 (bottom). The two $edte^{4-}$ groups each bind as hexadentate chelates on a Mn^{II} atom (Mn1) and bridge with their alkoxide arms to either one or two adjacent Mn^{III} atoms to give the overall $\eta^1{:}\eta^1{:}\eta^2{:}\eta^3{:}\eta^3{:}\eta^3{:}\mu_6$ binding mode shown in Figure 5. The two Mn2···Mn5 edges are also each bridged by a μ-OMe^- group. Peripheral ligation at each Mn_{10} is completed by six bridging $EtCO_2^-$ groups and six azide groups. The Mn oxidation states and O protonation levels were confirmed by BVS calculations (Tables 3 and 4); the Mn^{II} and Mn^{III} are seven- and six-coordinate, respectively.

The Mn_{10} units are bridged into a chain polymer by the Na^+ ions attaching at each end of the Mn_{10} unit to a cubane O^{2-}, bridging $EtCO_2^-$ and azide groups, and the latter bridges in an end-to-end fashion to the Na^+ on an adjacent unit to give the polymer; the unit connecting repeating units is thus $[Na_2(\mu\text{-}N_3^-)_2]$ (Supporting Information, Figure S3).[22] Octahedral coordination at each Na^+ is then completed by terminal MeCN and MeOH groups.

The partially labeled structure of $(NEt_4)_2[Mn_{10}(O)_4(OH)_2\text{-}(O_2CEt)_6(edte)_2(N_3)_6]$ (**5**) and a stereoview are presented in

dx.doi.org/10.1021/ic201916d | Inorg. Chem. 2011, 50, 12774–12784

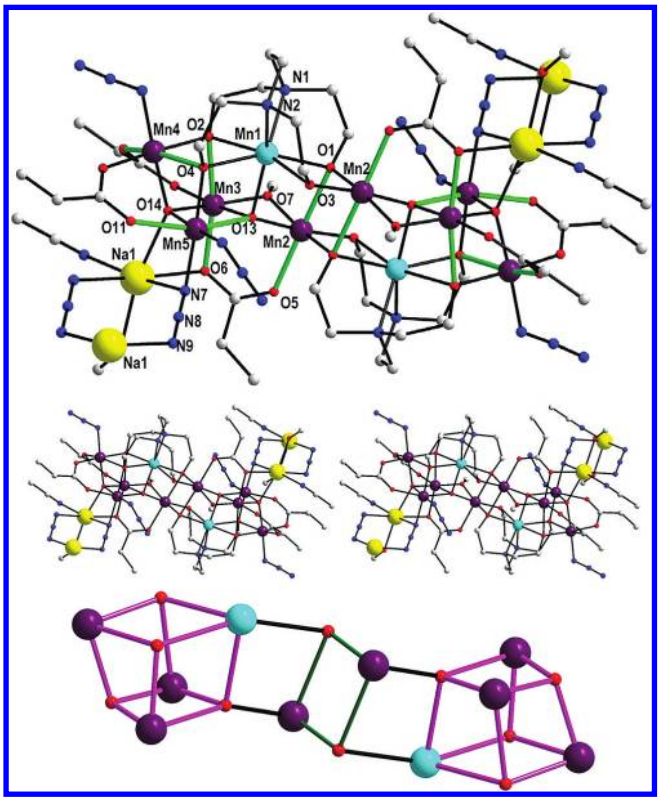

Figure 4. Portion of the polymeric structure of **4** (top), a stereopair (middle), and the core (bottom). The Mn^{III} JT axes are shown as green lines. H atoms have been omitted for clarity. Color code: Mn^{III}, purple; Mn^{II}, cyan; Na, yellow; O, red; N, blue; C, light gray.

Figure 6, and selected interatomic distances and angles are listed in Table 7. The core of centrosymmetric **5** is very similar to that of **4**, except that it contains a discrete Mn_{10} cluster dianion and two NEt_4^+ cations. The Mn oxidation states and O protonation levels (Tables 3 and 4) are also the same as in **4**. There is, however, one other major difference between **4** and **5**, and that is the replacement of the two μ-OMe^- groups in **4** with μ-OH^- groups in **5**, undoubtedly because of hydrolysis. Complex **5** joins a small family of discrete Mn_{10} complexes in the literature.[31] These possess a variety of metal topologies, but none of them have possessed the core of complex **5**, which is unprecedented.

It is interesting to note that the cores of complexes **2**–**5** are related by the fact that they all contain a Mn_4 rhombus, either alone (**2**) or as the central unit with one (**3**) or three (**4**, **5**) additional Mn atoms connected at each end. In fact, the core of **2** can even be related to that of **1**, because it can be thought of as the addition of an extra Mn at the central position.

Magnetochemistry. Solid-state, variable-temperature dc magnetic susceptibility data were collected in a 1000 G (0.1 T) field and in the 5.0–300 K range on powdered microcrystalline samples of **1**·H_2O, **2**, **3**, **4**·$2H_2O$, and **5**·H_2O restrained in solid eicosane to avoid torquing. For **1**·H_2O, $\chi_M T$ slowly decreases from 10.98 cm^3 K mol^{-1} at 300 K to 5.79 cm^3 K mol^{-1} at 5 K. This suggests the presence of antiferromagnetic exchange interactions and an $S = 3$ ground state with g slightly <2.0; the spin-only ($g = 2$) value for $S = 3$ is 6.0 cm^3 K mol^{-1}. The data for complex **1** were fit to the theoretical $\chi_M T$ vs T expression for a linear $Mn^{II}Mn^{III}Mn^{II}$ core with two exchange coupling

Table 6. Selected Interatomic Distances (Å) and Angles (deg) for 4·2MeCN

Mn(1)···Mn(2′)	3.218(1)	Mn(3)···Mn(5)	3.089(1)
Mn(1)···Mn(2)	3.245(1)	Mn(3)···Na(1)	3.276(1)
Mn(1)···Mn(3)	3.224(1)	Mn(3)···Mn(4)	2.955(1)
Mn(1)···Mn(4)	3.541(1)	Mn(4)···Mn(5)	3.023(1)
Mn(2)···Mn(3)	2.843(1)	Mn(5)...Na(1)	3.438(1)
Mn(2)···Mn(2′)	3.311(1)	Mn(5)...Mn(1)	3.269(1)
Mn(1)−O(3)	2.205(2)	Mn(3)−O(7)	1.943(2)
Mn(1)−O(1)	2.237(2)	Mn(3)−O(13)	1.873(2)
Mn(1)−O(4)	2.243(2)	Mn(3)−O(14)	1.916(2)
Mn(1)−O(2)	2.364(2)	Mn(4)-O(2′)	1.950(2)
Mn(1)-O(13′)	2.214(2)	Mn(4)-O(4′)	2.318(2)
Mn(2)−O(1)	1.938(2)	Mn(4)−O(14)	1.909(3)
Mn(2)−O(7)	1.963(2)	Mn(5)−O(13)	2.345(2)
Mn(2)−O(13)	1.902(2)	Mn(5)−O(14)	1.939(2)
Mn(3)-O(2′)	2.254(2)	Mn(5)-O(4′)	1.953(2)
Mn2−O1−Mn1	100.65(8)	Mn3−O13−Mn2	97.75(9)
Mn2−O1−Mn2′	101.06(8)	Mn3−O13−Mn1′	103.83(8)
Mn1−O1−Mn2′	90.29(7)	Mn2−O13−Mn1′	103.77(9)
Mn4′−O2-Mn1	109.99(8)	Mn3−O13−Mn5	93.51(8)
Mn3′−O2-Mn1	88.53(6)	Mn2−O13−Mn5	158.11(10)
Mn2−O3−Mn1	103.41(9)	Mn4−O14−Mn3	101.16(9)
Mn5′−O4-Mn1	102.14(8)	Mn4−O14−Mn5	103.54(9)
Mn5′−O4-Mn4′	89.68(8)	Mn3−O14−Mn5	106.54(9)
Mn1−O4−Mn4′	101.86(8)	Mn4−O14−Na1	141.69(10)
Mn3−O7−Mn2	93.46(8)	Mn3−O14−Na1	97.05(8)
Mn1′−O13-Mn5	91.58(7)	Mn5−O14−Na1	103.11(8)

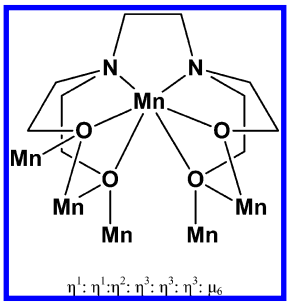

Figure 5. μ_6 ligation mode of the $edte^{4-}$ group in **4**.

parameters, J and J', representing the $Mn^{II}Mn^{III}$ and $Mn^{III}Mn^{III}$ interactions, respectively. The corresponding Heisenberg spin Hamiltonian is given by eq 6 (the atom labeling as in Figure 1) and its eigenvalues in eq 7, where $\hat{S}_A = \hat{S}_1 + \hat{S}_{1'}$, $\hat{S}_T = \hat{S}_A + \hat{S}_2$, and S_T is the total spin of the molecule.

$$\hat{H} = -2J(\hat{S}_1 \cdot \hat{S}_2 + \hat{S}_{1'} \cdot \hat{S}_2) - 2J'\hat{S}_1 \cdot \hat{S}_{1'} \quad (6)$$

$$E(S_T, S_A) = -J[S_T(S_T + 1) - S_A(S_A + 1)] - J'[S_A(S_A + 1)] \quad (7)$$

Equation 7 and the Van Vleck equation were used to derive the theoretical $\chi_M T$ vs T expression for **1**·H_2O, and this was used to least-squares-fit the experimental data. The fit (solid line in Figure 7) gave $J = -1.4(1)$ cm^{-1}, $J' = 0.3(1)$ cm^{-1}, and $g = 1.98(1)$. These values identify $|S_T, S_A\rangle = |3, 5\rangle$ as the ground state, as expected. There are 24 possible S_T states ranging in value from 0 to 7, and the S_T energy diagram is shown in Supporting Information, Figure S4.[22] The first and second

dx.doi.org/10.1021/ic201916d | Inorg. Chem. 2011, 50, 12774–12784

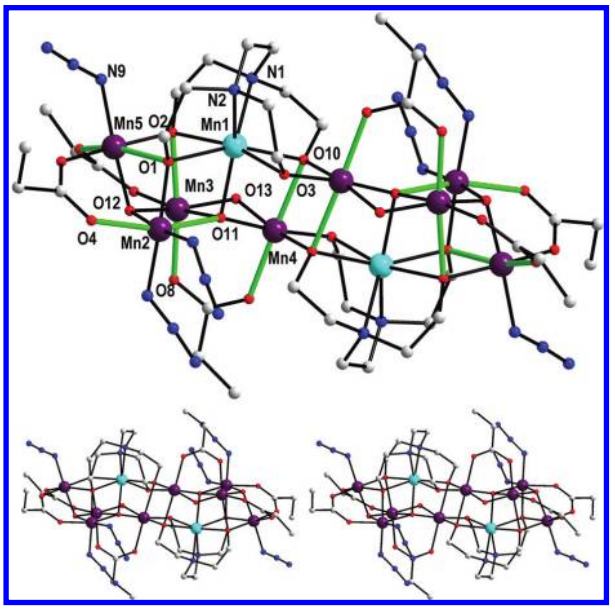

Figure 6. Structure of the cation of **5** (top), and a stereopair (bottom). H atoms have been omitted for clarity. Color code: Mn^{III}, purple; Mn^{II}, cyan; O, red; N, blue; C, light gray.

Table 7. Selected Interatomic Distances (Å) and Angles (deg) for 5·2MeCN

Mn(1)···Mn(2′)	3.283(1)	Mn(3)···Mn(4)	2.861(1)
Mn(1)···Mn(4)	3.242(1)	Mn(3)···Mn(5)	2.986(1)
Mn(2)···Mn(3)	3.079(1)	Mn(4)···Mn(1′)	3.225(1)
Mn(5)···Mn(2)	3.014(1)	Mn(1)···Mn(4′)	3.225(1)
Mn(5)···Mn(3)	2.986(1)	Mn(3)···Mn(1)	3.254(1)
Mn(1)−O(3)	2.190(2)	Mn(3)−O(12)	1.907(2)
Mn(1)−O(11)	2.213(2)	Mn(3)−O(13)	1.995(2)
Mn(1)−O(1)	2.237(2)	Mn(4)-O(3#1)	1.886(2)
Mn(1)−O(10)	2.251(2)	Mn(4)−O(11)	1.892(2)
Mn(1)−O(2)	2.350(2)	Mn(4)-O(10′)	1.956(2)
Mn(2)−O(1)	1.978(2)	Mn(4)−O(13)	1.993(2)
Mn(2)−O(11)	2.356(2)	Mn(4)−O(10)	2.315(2)
Mn(2)−O(12)	1.923(2)	Mn(5)−O(12)	1.897(2)
Mn(3)−O(11)	1.872(2)	Mn(5)−O(2)	1.958(2)
Mn2−O1−Mn1	102.16(8)	Mn(5)−O(1)	2.297(2)
Mn2−O1−Mn5	89.33(8)	Mn3−O11−Mn4	98.95(9)
Mn1−O1−Mn5	101.06(8)	Mn3−O11−Mn1	105.29(9)
Mn5−O2−Mn3	88.84(7)	Mn4−O11−Mn1	104.06(9)
Mn5−O2−Mn1	108.39(9)	Mn3−O11−Mn2	92.77(8)
Mn3−O2−Mn1	88.95(7)	Mn4−O11−Mn2	156.88(11)
Mn4′−O3-Mn1	104.38(9)	Mn1−O11−Mn2	91.83(7)
Mn4′−O10-Mn1	99.87(8)	Mn5−O12−Mn3	103.44(9)
Mn4−O13−Mn3	91.69(9)	Mn5−O12−Mn2	104.16(10)
Mn1−O10−Mn4	90.48(7)	Mn3−O12−Mn2	107.01(9)

excited states are |2, 4⟩ and |4, 5⟩ at 8.6 and 11.3 cm^{-1}, respectively, above the ground state.

Variable-field (H) and -temperature magnetization (M) data were collected on **1**·H_2O in the 0.1−7 T and 1.8−10 K ranges, and they are plotted as reduced magnetization ($M/N\mu_B$) vs H/T (N is Avogadro's number) in Figure 8. The data were fit using the program MAGNET,[16] by diagonalization of the spin Hamiltonian matrix assuming only the ground state is populated, incorporating axial anisotropy ($D\hat{S}_z^2$) and Zeeman terms, and employing a full powder average. The corresponding

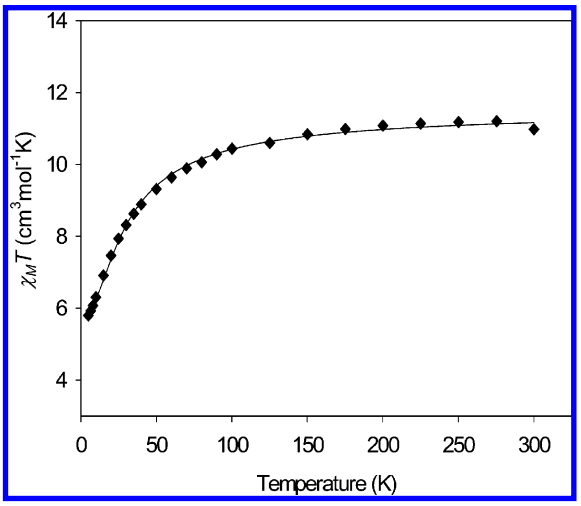

Figure 7. $\chi_M T$ vs T plot for **1**·H_2O. The solid line is the fit of the data; see the text for the fit parameters.

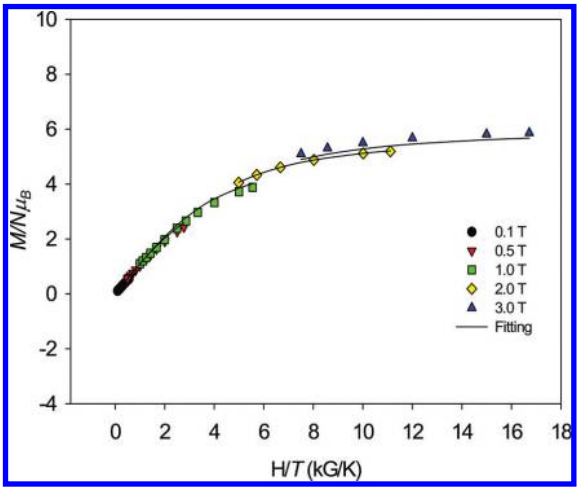

Figure 8. Plot of reduced magnetization ($M/N\mu_B$) vs H/T for complex **1**·H_2O in dc fields of 0.1−3.0 T in the 1.8−10 K range. The solid lines are the fit to the data; see the text for the fit parameters.

spin Hamiltonian is given by the eq 8 where $\hat{S}_z$ is the easy-axis spin operator, μ_B is the Bohr magneton, and μ_0 is the vacuum permeability. A reasonable fit was obtained, but only if data collected at the highest fields were omitted. This is typical of Mn^{II}-containing species where excited states are relatively low-lying;[32] in the present case, we could include data up to 30 kG (3 T) fields.

$$H = D\hat{S}_z^2 + g\mu_B\mu_0\hat{S}\cdot H \quad (8)$$

The fit is shown as the solid lines in Figure 8, and the fit parameters were $S = 3$, $g = 2.03(1)$, and $D = -0.38(4)$ cm^{-1}. The complete data collected in fields up to 7 T are shown in Supporting Information, Figure S8.[22] Alternative fits were also obtained with $S = 2$, $g = 2.93$ and $S = 4$, $g = 1.57$, but were discarded because of the unreasonable g values. The fitting was also acceptable with $S = 3$, $g = 2.02(1)$, and $D = 0.37(6)$ cm^{-1}. The root-mean-square D vs g error surface for the fit (Supporting Information, Figure S5), generated using the program GRID,[33] showed the fit with negative D to be superior.

dx.doi.org/10.1021/ic201916d | Inorg. Chem. 2011, 50, 12774–12784

As an independent probe of the ground state, ac susceptibility data were collected for **1**·H_2O in the 1.8−15 K range using a 3.5 G ac field oscillating at frequencies in the 50−1000 Hz range. The obtained in-phase (χ'_M, plotted as χ'_MT) ac susceptibility data are shown in Figure 9. χ'_MT is decreasing in

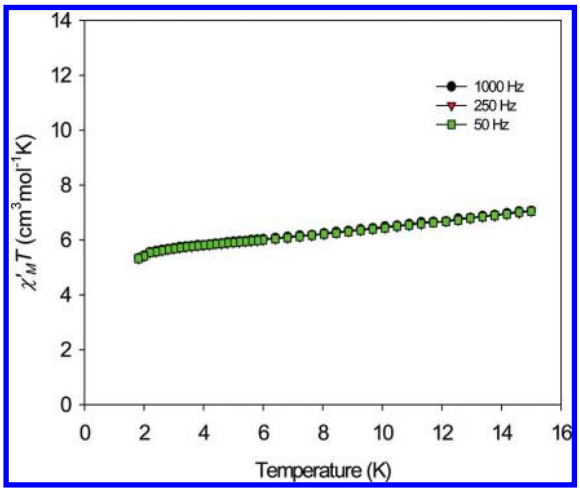

Figure 9. In-phase ac susceptibility, χ'_M (as χ'_MT) vs T in the 1.8−15 K range for **1**·H_2O at the indicated frequencies.

this temperature range and heading for a value of ∼5.8 cm^3 K mol^{-1} at 0 K, as expected for an S = 3 ground state and g slightly less than 2, before a small dip below 2.5 K because of weak intermolecular interactions or ZFS.

For complex **2**, χ_MT is 18.18 cm^3 K mol^{-1} at 300 K and increases steadily with decreasing temperature to a maximum of 41.58 cm^3 K mol^{-1} at 6.5 K, suggestive of an S = 9 ground state, before decreasing very slightly because of ZFS, interion interactions and/or Zeeman effects (Figure 10). The χ_MT values have been

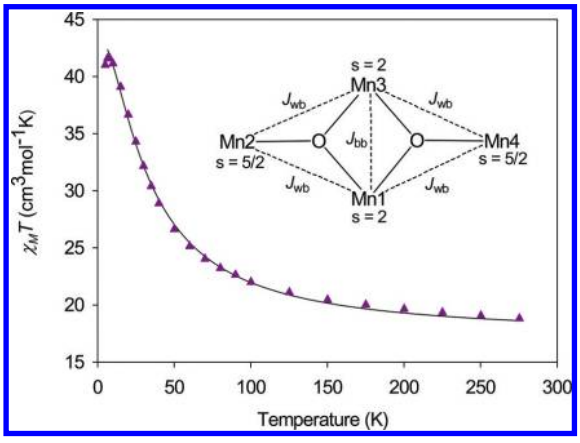

Figure 10. χ_MT vs T data for **2**. The solid line is the fit of the data to the 2-J coupling model shown as the inset; see the text for the fit parameters.

reduced by 4.375 cm^3 K mol to remove the contribution of the $MnCl_4^{2-}$ anion. The spin Hamiltonian for a Mn_4 rhombus is given by eq 9 (atom labeling as in the inset to Figure 10; Mn1 = Mn3 = Mn^{III} and Mn2 = Mn4 = Mn^{II}), where J_{wb} and J_{bb} are the $Mn^{II}Mn^{III}$ and $Mn^{III}Mn^{III}$ interactions, respectively.

$$\hat{H} = -2J_{wb}(\hat{S}_1\cdot\hat{S}_2 + \hat{S}_1\cdot\hat{S}_4 + \hat{S}_2\cdot\hat{S}_3 + \hat{S}_3\cdot\hat{S}_4) - 2J_{bb}\hat{S}_1\cdot\hat{S}_3 \quad (9)$$

The eigenvalues of eq 9 are given by eq 10, where $\hat{S}_A = \hat{S}_1 + \hat{S}_3$, $\hat{S}_B = \hat{S}_2 + \hat{S}_4$, $\hat{S}_T = \hat{S}_A + \hat{S}_B$, S_T is the total spin of the molecule, and $E|S_T, S_A, S_B\rangle$ is the energy of state S_T arising from particular S_A and S_B.[34]

$$E|S_T, S_A, S_B\rangle = -J_{wb}[S_T(S_T+1) - S_A(S_A+1) - S_B(S_B+1)] - J_{bb}[S_A(S_A+1)] \quad (10)$$

There are 110 S_T states ranging in value from 0 to 9, and these, together with eq 10 and the Van Vleck equation, were used to derive a theoretical χ_MT vs T expression that was used to fit the data in the 6.5−300 K range.[35] The fit (solid line in Figure 10) gave J_{bb} = +7.20(3) cm^{-1}, J_{wb} = +1.34(3) cm^{-1}, and g = 1.87(2), with temperature-independent paramagnetism (TIP) fixed at 600 × 10^{-6} cm^3 mol^{-1}. The low g value is an artifact reflecting the low reliability of g values from powder susceptibility fits; a value only slightly below 2.0 is expected. The fit values identify a $|S_T, S_A, S_B\rangle$ = |9, 4, 5⟩ ground-state for **2**, and the complete S_T energy diagram is shown in Supporting Information, Figure S6.[22] The first two excited states are |8, 4, 4⟩ and |7, 4, 3⟩ at 10.72 and 21.44 cm^{-1}, respectively, above the ground state.

The ac in-phase χ'_MT for **2** slowly rises from 40.49 cm^3 K mol^{-1} at 15 K to a maximum of 43.12 cm^3 K mol^{-1} at ∼7 K consistent with an S = 9 ground state, but then decreases sharply to 37.98 cm^3 K mol^{-1} at 1.8 K (Figure 11). The decrease is not frequency-

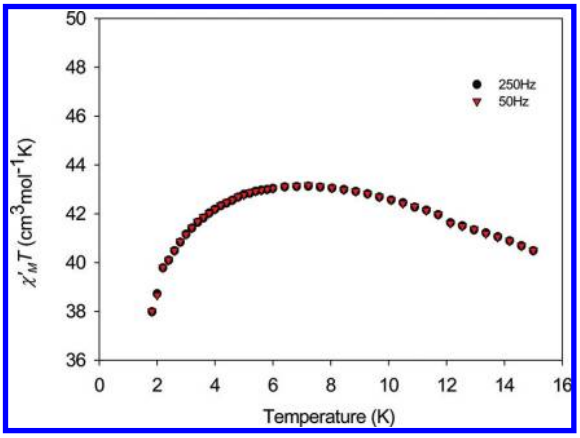

Figure 11. In-phase ac susceptibility, χ'_M (as χ'_MT) vs T in the 1.8−15 K range for **2** at the indicated frequencies.

dependent and it is thus attributed to interion antiferromagnetic interactions between Mn_4 cations and $MnCl_4^{2-}$ anions propagated primarily by the OH···Cl hydrogen-bonds seen in the crystal structure that give chains (Supporting Information, Figure S2).[22] Discrete Mn_4 complexes of this structural type with S = 9 ground states are well studied members of the SMM family,[36] but the absence of a frequency-dependent decrease in χ'_MT (or a frequency dependent out-of-phase signal, $\chi_M''T$) indicates the hydrogen-bonded chain **2** not to exhibit particularly slow relaxation, above 1.8 K at least, and its study at lower temperatures was therefore not pursued.

For complex **3**, χ_MT is 16.97 cm^3 K mol^{-1} at 300 K, and steadily decreases with decreasing temperature to a minimum value of 7.76 cm^3 K mol^{-1} at 10 K, below which there is a small increase to 7.87 cm^3 K mol^{-1} at 5.0 K (Figure 12). The near-plateau value below 10 K would seem to suggest a well isolated ground state of S = 4 but with a very low g = 1.77, much too low for a Mn^{III} complex; spin-only (g = 2) values for S = 3, 4, and 5 systems are 6.0, 10.0, and 15 cm^3 K mol^{-1}. The ground state was probed further by fits of magnetization (M) data collected in the 0.1−7 T and 1.8−10 K field (H) and temperature

dx.doi.org/10.1021/ic201916d | Inorg. Chem. 2011, 50, 12774−12784

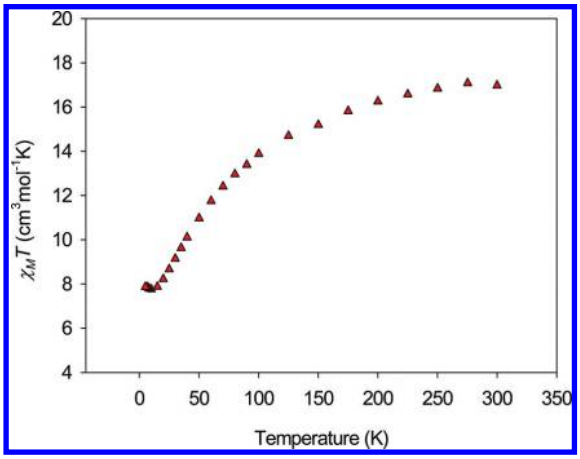

Figure 12. $\chi_M T$ vs T plot for **3**.

ranges, respectively. The data are plotted as reduced magnetization ($M/N\mu_B$) vs H/T in Figure 13, and the best-fit gave $S = 4$,

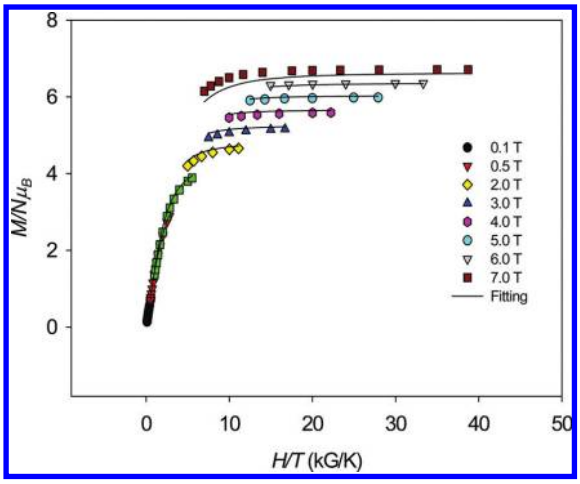

Figure 13. Plot of reduced magnetization ($M/N\mu_B$) vs H/T for **3** in dc fields of 0.1−7.0 T in the 1.8−10 K range. The solid lines are the fit to the data; see the text for the fit parameters.

$D = -1.06(15)$ cm^{-1}, and $g = 1.88(4)$. The low precision on D and g are reflected in the fit error surface (Supporting Information, Figure S7), which exhibits an unusual and very soft fit minimum, showing in effect that a range of combinations of D and g gives similar quality fits of the data. Alternative fits were obtained with $S = 3$, $g = 2.48$ and $S = 5$, $g = 1.52$, but were discarded because of the unreasonable g values. In the ac data for **3**, $\chi'_M T$ is almost temperature-independent below 10 K at a value of ∼8.0 cm^3 K mol^{-1}, with a very slight increase as the temperature decreases (Figure 14). This completely agrees with the dc data, indicating an $S = 4$ ground state with $g \sim 1.78$.

The $S = 4$ ground state is considered reasonable on the basis of the structure (Figure 3). If each Mn^{III}_2 pair bridged by two monatomic bridges (central Mn3Mn3 and the two Mn1Mn2 pairs) are ferromagnetically coupled, as is the Mn^{III}_2 pair in **2**, and interactions between these pairs through single monatomic bridges are antiferromagnetic (as expected), then an $S = 4$ ground is predicted. The data, however, makes us disfavor the conclusion that the ground state is well isolated: (i) the g values suggested by the dc $\chi_M T$ vs T and $M/N\mu_B$ vs H/T fits and the ac $\chi'_M T$ data are all worryingly low; (ii) the $|D|$ value from the $M/N\mu_B$ vs H/T fit is unusually large; (iii) the $M/N\mu_B$ vs H/T

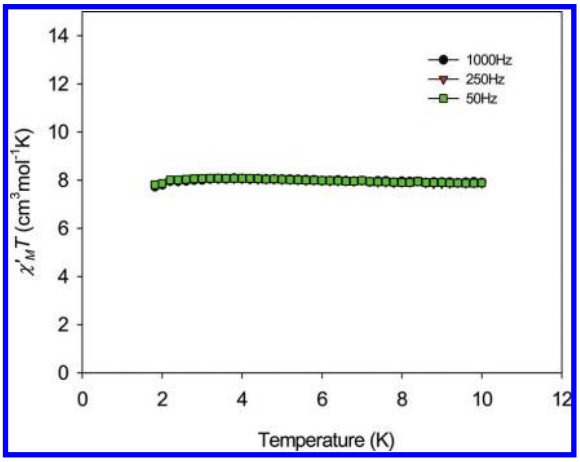

Figure 14. In-phase ac susceptibility, χ'_M (as $\chi'_M T$) vs T in the 1.8−10 K range for **3** at the indicated frequencies.

fit is good, but not excellent as normally expected for a well isolated ground state; and (iv) the small but real increase in both the dc $\chi_M T$ and ac $\chi'_M T$ data at low T is intriguing. While any of these points by themselves could be rationalized as experimental error or similar, in combination we believe they are pointing to one or more very low-lying excited states, almost degenerate with the ground state. In this regard, we note that population of only the $S = 4$ ground state and an essentially degenerate $S = 3$ state (the most likely first excited state of **3**) would give a $\chi_M T$ of 7.88 cm^3 K mol^{-1} for $g = 2.0$, very close to the observed dc and ac values at low T. Then, (a) the small increase with decreasing T in the dc and ac plots would be due to small changes in $S = 4/S = 3$ relative populations, and (b) the large $|D|$ would be an artifact of two states being populated and contributing to the isofield lines not being superimposed, whereas the fitting procedure assumes only one is populated and thus assigns the nonsuperimposed lines wholly to $|D|$, giving an erroneously large value. Future work with high-frequency Electron Paramagnetic Resonance (EPR) spectroscopy will probe this possibility by determining the states populated at low T and their D values. We also note that a well isolated $S = 4$ with $D \approx -1.0$ cm^{-1} would give a calculated barrier (U) to magnetization relaxation of $U = S^2|D| = 16$ cm^{-1} = 23 K. Although the true barrier U_{eff} would be less than U because of tunneling effects, it might still be expected to be large enough to give out-of-phase (χ''_M) ac signals characteristic of a SMM. However, no χ''_M signals were observed for **3** down to 1.8 K, suggesting the true magnitude of $|D|$ is much smaller.

For complexes **4** and **5**, the $\chi_M T$ vs T profiles are overall similar, as expected from their similar structures, but with a few differences as well. $\chi_M T$ for **4** and **5** at 300 K are 29.49 and 30.62 cm^3 K mol^{-1}, and steadily decrease with decreasing temperature to 9.70 and 12.06 cm^3 K mol^{-1}, respectively, at 5.0 K (Figure 15). The profiles indicate predominantly antiferromagnetic interactions within the Mn_{10} clusters. For both complexes, we could not get acceptable fits of the magnetization data, even when only data collected at low fields were employed. We assign this to the large metal nuclearity of the complex and the presence of Mn^{II} atoms, which together will give a large density of very low-lying excited states. The ac data support the latter conclusion, showing steeply decreasing $\chi'_M T$ below 15 K as excited states are depopulated (Figure 16). The $\chi'_M T$ for discrete complex **5** appears to be heading to just under 10 cm^3 K mol^{-1}, which might be indicating an $S = 4$

dx.doi.org/10.1021/ic201916d | Inorg. Chem. 2011, 50, 12774–12784

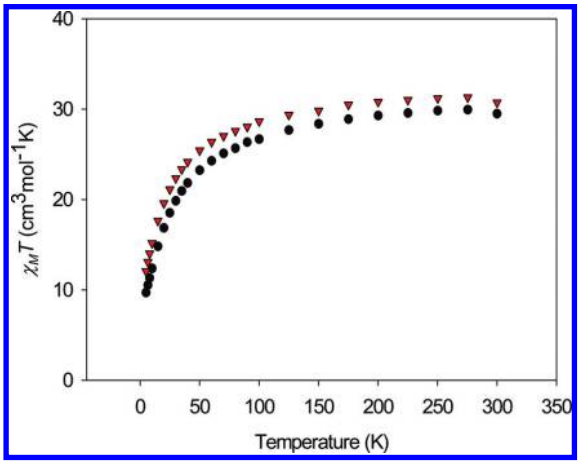

Figure 15. $\chi_M T$ vs T plots for **4**·2H_2O (●) and **5**·H_2O (▼).

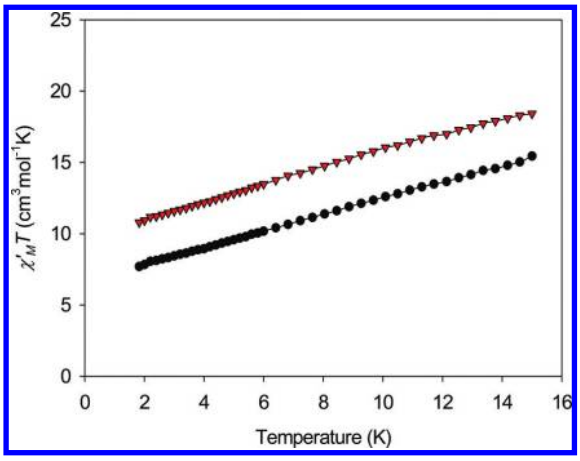

Figure 16. In-phase ac susceptibility, χ'_M (as $\chi'_M T$) vs T in the 1.8–15 K range for **4**·2H_2O (●) and **5**·H_2O (▼) at 1000 Hz.

ground state with g slightly less than 2.0. Polymer **4** shows slightly smaller $\chi'_M T$, which might be reflecting inter-Mn_{10} interactions but more likely just small differences in the intramolecular J values and resulting spin frustration effects from small differences in metric parameters, particularly Mn–O–Mn angles. Thus, probably the safest conclusion to draw is that both complexes have small ground states in the S = 0–4 range and several very low-lying excited states.

CONCLUSIONS

This work emphasizes once again the utility of the multidentate edteH_4 in its various deprotonated forms as a route to Mn clusters of widely differing nuclearities. This is facilitated by the ability of this group to bridge multiple metal atoms, in this work up to six. As a result, and depending on the exact reagent ratios and reaction conditions, the present work has led to Mn_x clusters spanning nuclearities from 3 to 10, but which nevertheless are structurally related in containing a similar central unit and varying numbers of additional Mn atoms at each end. These new complexes add to others with nuclearities up to 20 in previous work. Although none of the present or past complexes with edte$H_x^{(4-x)-}$ ligation have been SMMs, we have recently finally encountered new Mn SMMs with this chelating group. This will be reported in the near future.

ASSOCIATED CONTENT

Supporting Information

X-ray crystallographic files in CIF format for complexes **1**·MeCN, **2**, **3**, **4**·MeCN, and **5**·2MeCN. Crystal packing diagrams for **1**, **2**, and **4**. Error surfaces for the magnetization fits for **1** and **3**. This material is available free of charge via the Internet at http://pubs.acs.org.

AUTHOR INFORMATION

Corresponding Author

*Phone: +1-352-392-8314. Fax: +1-352-392-8757. E-mail: christou@chem.ufl.edu.

ACKNOWLEDGMENTS

We thank the National Science Foundation (CHE-0910472) for support of this work.

REFERENCES

(1) (a) Pecoraro, V. L. *Manganese Redox Enzymes*; VCH Publishers: New York, 1992. (b) Jiang, W.; Yun, D.; Saleh, L.; Barr, E. W.; Xing, G.; Hoffart, L. M.; Maslak, M.-A.; Krebs, C.; Bollinger, J. M. Jr. *Science* **2007**, *316*, 1188.

(2) (a) Barber, J.; Murray, J. W. *Coord. Chem. Rev.* **2008**, *252*, 233. (b) Barber, J. *Inorg. Chem.* **2008**, *47*, 1700.

(3) (a) Ferreira, K. N.; Iverson, T. M.; Maghlaoui, K.; Barber, J.; Iwata, S. *Science* **2004**, *303*, 1831. (b) Yano, J.; Kern, J.; Sauer, K.; Latimer, M.; Pushkar, Y.; Biesiadka, J.; Loll, B.; Saenger, W.; Messinger, J.; Zouni, A.; Yachandra, V. K. *Science* **2006**, *314*, 821. (c) Umena, Y.; Kawakami, K.; Shen, J.-R.; Kamiya, N. *Nature* **2011**, *473*, 55.

(4) (a) Ako, A. M.; Hewitt, I. J.; Mereacre, V.; Clérac, R.; Wernsdorfer, W.; Anson, C. E.; Powell, A. K. *Angew. Chem., Int. Ed.* **2006**, *45*, 4926. (b) Ge, C.-H.; Ni, Z.-H.; Liu, C.-M.; Cui, A.-L.; Zhang, D.-Q.; Kou, H.-Z. *Inorg. Chem. Commun.* **2008**, *11*, 675. (c) Moushi, E. E.; Stamatatos, Th. C.; Wernsdorfer, W.; Nastopoulos, V.; Christou, G.; Tasiopoulos, A. J. *Inorg. Chem.* **2009**, *48*, 5049. (d) Nayak, S.; Beltran, L. M. C.; Lan, Y.; Clérac, R.; Hearns, N. G. R.; Wernsdorfer, W.; Anson, C. E.; Powell, A. K. *Dalton Trans.* **2009**, 1901. (e) Stamatatos, Th. C.; Abboud, K. A.; Wernsdorfer, W.; Christou, G. *Angew. Chem., Int. Ed.* **2007**, *46*, 884.

(5) Kahn, O. *Molecular Magnetism*; VCH Publishers: New York, 1993.

(6) (a) Bagai, R.; Christou, G. *Chem. Soc. Rev.* **2009**, *38* (4), 1011 , and references cited therein. (b) Christou, G.; Gatteschi, D.; Hendrickson, D. N.; Sessoli, R. *MRS Bull.* **2000**, *25*, 66. (c) Aromi, G.; Brechin, E. K. *Struct. Bonding (Berlin)* **2006**, *122*, 1. (d) Bircher, R.; Chaboussant, G.; Dobe, C.; Gudel, H. U.; Ochsenbein, S. T.; Sieber, A.; Waldmann, O. *Adv. Funct. Mater.* **2006**, *16*, 209. (e) Gatteschi, D.; Sessoli, R. *Angew. Chem., Int. Ed.* **2003**, *42*, 268.

(7) Karotsis, G.; Kennedy, S.; Teat, S. J.; Beavers, C. M.; Fowler, D. A.; Morales, J. J.; Evangelisti, M.; Dalgarno, S. J.; Brechin, E. K. *J. Am. Chem. Soc.* **2010**, *132*, 12983.

(8) (a) Taguchi, T.; Daniels, M. R.; Abboud, K. A.; Christou, G. *Inorg. Chem.* **2009**, *48*, 9325. (b) Taguchi, T.; Wernsdorfer, W.; Abboud, K. A.; Christou, G. *Inorg. Chem.* **2010**, *49*, 199. (c) Taguchi, T.; Wernsdorfer, W.; Abboud, K. A.; Christou, G. *Inorg. Chem.* **2010**, *49*, 10579.

(9) (a) Hundal, G.; Hundal, M. S.; Obrai, S.; Poonia, N. S.; Kumar, S. *Inorg. Chem.* **2002**, *41*, 2077. (b) Plass, W. *Eur. J. Inorg. Chem.* **1998**, 799. (c) de Sousa, A. S.; Fernandes, M. A. *Polyhedron* **2002**, *21*, 1883.

(10) (a) Bagai, R.; Abboud, K. A.; Christou, G. *Inorg. Chem.* **2008**, *47*, 621. (b) Zhou, A. J.; Qin, L. J.; Beedle, C. C.; Ding, S.; Nakano, M.; Leng, J. D.; Tong, M. L.; Hendrickson, D. N. *Inorg. Chem.* **2007**, *46*, 8111. (c) Zhou, A.-J.; Liu, J.-L.; Herchel, R.; Leng, J.-D.; Tong, M.-L. *Dalton Trans.* **2009**, 3182.

(11) Bagai, R.; Daniels, M. R.; Abboud, K. A.; Hill, S.; Christou, G. *Inorg. Chem.* **2008**, *47*, 3318.

(12) Tasiopoulos, A. J.; Abboud, K. A.; Christou, G. *Chem. Commun.* **2003**, 580.
(13) Yu, S. B.; Shweky, I.; Lippard, S. J.; Bino, A. *Inorg. Chem.* **1992**, *31*, 3502.
(14) Lis, T. *Acta Crystallogr., Sect. B* **1977**, *33*, 2964.
(15) Vandersluis, P.; Spek, A. L. *Acta Crystallogr., Sect. A* **1990**, *46*, 194.
(16) Davidson, E. R. *MAGNET*; Indiana University: Bloomington, IN, 1999.
(17) (a) Murugesu, M.; Wernsdorfer, W.; Abboud, K. A.; Christou, G. *Angew. Chem., Int. Ed.* **2005**, *44*, 892. (b) Cañada-Vilalta, C.; Pink, M.; Christou, G. *Dalton Trans.* **2003**, 1121.
(18) Taguchi, T.; Wernsdorfer, W.; Abboud, K. A.; Christou, G. *Inorg. Chem.* **2010**, *49*, 199.
(19) (a) Stamatatos, T. C.; Christou, G. *Inorg. Chem.* **2009**, *48*, 3308−3322, (references cited therein). (b) Stamatatos, T. C.; Abboud, K. A.; Wernsdorfer, W.; Christou, G. *Angew. Chem., Int. Ed.* **2008**, *47*, 6694. (c) Stamatatos, T. C.; Vinslava, A.; Abboud, K. A.; Wernsdorfer, W.; Christou, G. *Chem. Commun.* **2009**, 2839. (d) Moushi, E. E.; Masello, A.; Wernsdorfer, W.; Nastopoulos, V.; Christou, G.; Tasiopoulos, A. J. *Dalton Trans.* **2010**, *39*, 4978. (e) Taguchi, T.; Wernsdorfer, W.; Abboud, K. A.; Christou, G. *Inorg. Chem.* **2010**, *49*, 10579.
(20) Stamatatos, T. C.; Vinslava, A.; Abboud, K. A.; Christou, G. *Chem. Commun.* **2009**, 2839.
(21) Brese, N. E.; O'keeffe, M. *Acta Crystallogr.* **1991**, *B47*, 192.
(22) See Supporting Information.
(23) Prescimone, A.; Wolowska, J.; Rajaraman, G.; Parsons, S.; Wernsdorfer, W.; Murugesu, M.; Christou, G.; Piligkos, S.; McInnes, E. J. L.; Brechin, E. K. *Dalton Trans.* **2007**, 5282.
(24) Yoshino, A.; Miyagi, T.; Asato, E.; Mikuriya, M.; Sakata, Y.; Sugiura, K.; Iwasaki, K.; Hino, S. *Chem. Commun.* **2000**, 1475.
(25) Higgs, T. C.; Spartalian, K.; O'Connor, C. J.; Matzanke, B. F.; Carrano, C. J. *Inorg. Chem.* **1998**, *37*, 2263.
(26) Hureau, C.; Anxolabéhère-Mallart, E.; Blondin, G.; Rivière, E.; Nierlich, M. *Eur. J. Inorg. Chem.* **2005**, 4808.
(27) Mukherjee, C.; Weyhermüller, T.; Wieghardt, K.; Chaudhuri, P. *Dalton Trans.* **2006**, 2169.
(28) Bhaduri, S.; Pink, M.; Christou, G. *Chem. Commun.* **2002**, 2352.
(29) (a) Milios, C. J.; Inglis, R.; Vinslava, A.; Bagai, R.; Wernsdorfer, W.; Parsons, S.; Perlepes, S. P.; Christou, G.; Brechin, E. K. *J. Am. Chem. Soc.* **2007**, *129*, 12505. (b) Inglis, R.; Dalgarno, S. J.; Brechin, E. K. *Dalton Trans.* **2010**, *39*, 4826.(b).
(30) (a) Rajaraman, G.; Murugesu, M.; Sañudo, E.-C.; Soler, M.; Wernsdorfer, W.; Helliwell, M.; Muryn, C.; Raftery, J.; Teat, S.-J.; Christou, G.; Brechin, E.-K. *J. Am. Chem. Soc.* **2004**, *126*, 15445. (b) Rajaraman, G.; Murugesu, M.; Sañudo, E. C.; Soler, M.; Wernsdorfer, W.; Helliwell, M.; Muryn, C.; Raftery, J.; Teat, S. J.; Christou, G.; Brechin, E. K. *J. Am. Chem. Soc.* **2004**, *126*, 15445. (c) Schake, A. R.; Vincent, J. B.; Li, Q.; Boyd, P. D. W.; Folting, K.; Huffman, J. C.; Hendrickson, D. N.; Christou, G. *Inorg. Chem.* **1989**, *28*, 1915−1923.
(31) (a) Langley, S. K.; Moubaraki, B.; Berry, K. J.; Murray, K. S. *Dalton Trans.* **2010**, *39*, 4848. (b) Moushi, E. E.; Lampropoulos, C.; Wernsdorfer, W.; Nastopoulos, V.; Christou, G.; Tasiopoulos, A. J. *Inorg. Chem.* **2007**, *46*, 3795. (c) Papatriantafyllopoulou, C.; Raptopoulou, C. P.; Escuer, A.; Milios, C. J. *Inorg. Chim. Acta* **2007**, *360*, 61. (d) Dou, J.; Liu, M.; Li, D.; Wang, D. *Eur. J. Inorg. Chem.* **2006**, 4866. (e) Goldberg, D. P.; Caneschi, A.; Delfs, C. D.; Sessoli, R.; Lippard, S. J. *J. Am. Chem. Soc.* **1995**, *117*, 5789. (f) Eppley, H. J.; Aubin, S. J. M.; Streib, W. E.; Bollinger, J. C.; Hendrickson, D. N.; Christou, G. *Inorg. Chem.* **1997**, *36*, 109. (g) Stamatatos, T. C.; Abboud, K. A.; Wernsdorfer, W.; Christou, G. *Angew. Chem., Int. Ed.* **2006**, *45*, 4134.
(32) (a) Soler, M.; Wernsdorfer, W.; Folting, K.; Pink, M.; Christou, G. *J. Am. Chem. Soc.* **2004**, *126*, 2156. (b) Sañudo, E. C.; Wernsdorfer, W.; Abboud, K. A.; Christou, G. *Inorg. Chem.* **2004**, *43*, 4137.
(33) Davidson, E. R. *GRID*; Indiana University: Bloomington, IN, 1999.
(34) Kambe, K. *J. Phys. Soc. Jpn.* **1950**, *5*, 48.
(35) Yang, E.-C.; Harden, N.; Wernsdorfer, W.; Zakharov, L.; Brechin, E. K.; Rheingold, A. L.; Christou, G.; Hendrickson, D. N. *Polyhedron* **2003**, *22*, 1857.
(36) Roubeau, O.; Clérac, R. *Eur. J. Inorg. Chem.* **2008**, 4325 , and references therein.